

# Estimating Maximum Aircraft Icing Environments Using a Large Data Base of In-Situ Observations

Stewart G. Cober\* and George A. Isaac†  
*Environment Canada, Toronto, Ontario, Canada, M3H 5T4*

A large data base of in-situ aircraft icing observations collected during five field campaigns with two research aircraft is used to assess the 99 and 99.9% liquid water content (LWC) values associated with icing environments. Icing environments assessed include those with drops smaller than 100  $\mu\text{m}$  and those with supercooled large drops (SLD) larger than 100  $\mu\text{m}$ . The low probability LWC values were calculated using an extreme value analysis technique, and the results were compared to those obtained by assuming that the LWC observations could be fitted to exponential, gamma or Weibull distributions. Extreme value analysis allows quantification of the nature of distributions in the tails of the distributions, and hence provides a more accurate method for determining extreme values and their associated confidence limits. The results are compared to the icing envelopes from the Federal Aviation Administration Regulation 25 Appendix C and with other icing envelopes. Scale factors for computation of 99 and 99.9% LWC values for icing environments at horizontal length scales larger than 3 km are also determined.

## Nomenclature

AIRS I	First Alliance Icing Research Study
CFDE I	First Canadian Freezing Drizzle Experiment
CFDE III	Third Canadian Freezing Drizzle Experiment
Dmax	Maximum drop diameter
EVD	Extreme value distribution
FAA	Federal Aviation Administration
FAR 25-C	FAA Regulation 25 Appendix C
FIRE.ACE	First ISCCP Regional Experiment Arctic Cloud Experiment
FSSP	Forward scattering spectrometer probe
LWC	Liquid water content
MSC	Meteorological Service of Canada
MVD	Drop median volume diameter
NASA	National Aeronautics and Space Administration
NRC	National Research Council
PMS	Particle Measuring System
SF	Dimensionless scale factor
SLD	Supercooled large drop > 100 $\mu\text{m}$ in diameter
TWC	Total water content
ZLE	SLD icing environment with freezing drizzle drops 100-500 in diameter
ZRE	SLD icing environment with freezing rain drops > 500 $\mu\text{m}$ in diameter
2D-C	2D (mono) cloud probe
2D-G	2D (grey) cloud probe
2D-P	2D (mono) precipitation probe

---

\* Chief, Cloud Physics and Severe Weather Research Section, Science and Technology Branch, Environment Canada, 4905 Dufferin Street, Toronto, Ontario, Canada, M3H 5T4.

† Senior scientist, Cloud Physics and Severe Weather Research Section, Science and Technology Branch, Environment Canada, 4905 Dufferin Street, Toronto, Ontario, Canada, M3H 5T4.

## I. Introduction

The Federal Aviation Administration (FAA) Regulation 25 Appendix C<sup>1</sup> (FAR 25-C) provides a characterization of aircraft icing environments, with 99.9 percentile curves (i.e. envelopes) that incorporate temperature, droplet mean effective diameter (median volume diameter MVD) and liquid water content (LWC). The FAR 25-C icing curves were based on in-situ data collected in the 1940s (Jones and Lewis 1949<sup>2</sup>, Lewis and Bergun 1952<sup>3</sup>). Several icing cylinders of different diameter were used to infer the LWC and MVD of the observed icing environments. These 99.9% envelopes for continuous maximum (extreme) icing conditions were developed for a horizontal distance of 17.4 n mi (approximately 32.2 km). The envelopes physically represent a 0.1% exceedance probability for simultaneously exceeding the values of LWC (larger), MVD (larger) and temperature (colder). In order to extrapolate their data to estimate the 99.9% icing environments, Lewis and Bergun (1952)<sup>3</sup> followed Gumbel (1942)<sup>4</sup> and fitted the cumulative probability distributions of the observed LWC values to a distribution of the form:

$$P \propto \exp[-e^{-\alpha(x-\mu)}] \quad (1)$$

where P is the probability distribution function for x and  $\alpha$  and  $\mu$  are constants. The FAR 25-C envelopes only include MVD values up to 40  $\mu\text{m}$  because the multi-cylinder technique was not able to accurately infer larger MVD values. Regardless, Jones and Lewis (1949)<sup>2</sup> suggested that extreme freezing rain conditions could be represented by a drop MVD of 1000  $\mu\text{m}$ , LWC of 0.15  $\text{g m}^{-3}$ , and a horizontal extent > 100 km.

Masters (1984)<sup>5</sup> used a different data base of icing measurements to estimate the 99.9% icing environments for cloud conditions at altitudes less than 10,000 feet above ground level. He fitted the cumulative probability distributions of observed LWC values to a distribution of the form:

$$P \propto \exp[-\exp(-k \log(\alpha(x - \mu)))] \propto \exp[(\alpha(x - \mu))^{-k}] \quad (2)$$

where k,  $\alpha$  and  $\mu$  are constants. Equation 2 is a form of the Weibull distribution. Neither Lewis and Bergun (1952)<sup>3</sup> nor Masters (1984)<sup>5</sup> determined the precise nature of their LWC distributions in the regions of the distributions tails, which is where the assessment of extreme LWC values is made.

Extreme value statistical analysis (Coles 2001)<sup>6</sup> allows quantification of the nature of distributions in the tails of the distributions, and hence provides a more accurate method for determining extreme values, and their associated confidence limits. Extreme value analysis is based on the “three types theorem” of Fisher and Tippett (1928)<sup>7</sup> which states that there are only three types of distributions which can arise as limiting distributions of extremes in random samples. The Fisher Tippett theorem indicates that the asymptotic distribution of the maxima belongs to one of the three distributions regardless of the original distribution of the observed data. The three types of extreme value distributions can be combined into a single family known as the generalized extreme value distribution (EVD) (Coles 2001)<sup>6</sup> which is of the form:

$$P = \exp\left[-\left(1 + \xi \left(\frac{x - \mu}{\psi}\right)^{-1/\xi}\right)\right] \quad (3)$$

where  $\mu$  is called the location parameter,  $\psi$  is called the scale parameter and  $\xi$  is called the shape parameter. The nature of the tail of the distribution is determined by  $\xi$  and the three types of extreme value distributions are related to whether  $\xi = 0$  (Gumbel family),  $\xi > 0$  (Fréchet family) or  $\xi < 0$  (Weibull family) as follows:

$$P = \exp[-e^{-x}] \quad \text{when } \xi = 0 \quad -\infty < x < \infty \quad (4)$$

$$P = \exp[-x^{-\alpha}] \quad \text{when } \xi > 0 \quad \alpha = 1/\xi \quad 0 < x < \infty \quad (5)$$

$$P = \exp[-(-x)^\alpha] \quad \text{when } \xi < 0 \quad \alpha = -1/\xi \quad -\infty < x < 0 \quad (6)$$

The Gumbel family of distributions have “medium” tailed distributions and include normal, lognormal, exponential and gamma distributions. The Fréchet family of distributions have tails that are wider, or longer,

than the Gumbel family and include the Cauchy and the student-t distributions. The Weibull family of distributions have tails that are narrower, or shorter, than the Gumbel family and include the uniform and beta distributions.

There are several techniques for estimating the parameters associated with the EVD (Coles 2001)<sup>6</sup>. The technique of threshold selection is used here. This involved choosing a threshold value and then fitting a generalized Pareto distribution to all of the observations that exceed the threshold value. The distribution of values above a threshold can be approximated by a generalized Pareto distribution (Gencay et al. 2002)<sup>8</sup>. It can be shown that the generalized Pareto distribution is analogous to the EVD with both distributions having a similar form and the same shape parameter (Coles 2001)<sup>6</sup>. When choosing a threshold, care must be taken to balance the number of exceedances of the threshold with the number of data points necessary for a good fit. Choosing a low threshold will allow more data points for the fit but may incorporate data from the centre of the distribution, rather than from only the tail. Choosing a high threshold will better represent the tail however there may be insufficient data points for an adequate fit. Sensitivity studies are required to ensure that the choice of threshold provides results that are reasonable and robust.

Newton (1978)<sup>9</sup> described icing accumulation envelopes which represented the potential accumulations of ice on a 3-inch cylinder in  $\text{g cm}^{-2} \text{h}^{-1}$ . Increasing potential accumulation represents an increasing severity of icing, and hence a decreased probability of occurrence. The potential accumulation would depend entirely on the collision-collection efficiency of the hydrometeor spectrum which is mainly a function of aircraft speed and droplet size. However, for drops greater than approximately 50  $\mu\text{m}$  in diameter the collision efficiency would be essentially 1, and there would be no way to distinguish the accumulation associated with 100  $\mu\text{m}$  drops with that from 500  $\mu\text{m}$  or 1000  $\mu\text{m}$  drops. Since the Newton (1978)<sup>9</sup> potential accumulation curves are physically based, in contrast to parameterizations of icing envelopes using a statistical technique such as extreme value analysis, they are compared with the results of the statistical analysis.

## II. Field Projects

In-situ measurements of aircraft icing environments were made during five field projects conducted by the Meteorological Service of Canada (MSC) and the NASA-Glenn Icing Branch during the period from 1995 through 2000. These field projects are summarized in Table 1:

Table 1. Summary of field projects.

Project	Organization	Date
First Canadian Freezing Drizzle Experiment (CFDE I)	MSC	March 1995
Third Canadian Freezing Drizzle Experiment (CFDE III)	MSC	Dec 1997 – Feb 1998
First ISCCP Regional Experiment Arctic Cloud Experiment (FIRE.ACE)	MSC	April 1998
First Alliance Icing Research Study (AIRS I)	MSC	Dec 1999 – Feb 2000
First Alliance Icing Research Study (AIRS I)	NASA	Dec 1999
SLD Flight Research Study	NASA	Jan 1997 – Feb 1998

CFDE I was based out of St. John's Newfoundland and consisted of research flights into winter storms where freezing precipitation conditions were forecast to exist. Most flights were conducted over the North Atlantic Ocean, hence the environments observed were maritime in nature. CFDE I has been described by Isaac et al. (1999)<sup>10</sup>, Isaac et al. (2001)<sup>11</sup> and Cober et al. (2001)<sup>12</sup>. CFDE III and AIRS I were based out of Ottawa and the flights were targeted at environments where supercooled large drop (SLD) and/or high LWC conditions were forecast to exist. CFDE III flights were conducted over southern Ontario, southern Quebec, Lake Ontario and Lake Erie while AIRS I flights were concentrated over Mirabel Quebec. The environments observed can be considered continental in nature. CFDE III has been described by Isaac et al. (1999)<sup>10</sup>, Isaac et al. (2001)<sup>11</sup> and Cober et al. (2001)<sup>12</sup>. AIRS I has been described by Isaac et al. (2001)<sup>13</sup> and Cober et al. (2002)<sup>14</sup>. FIRE.ACE (Curry et al 2000)<sup>15</sup> was based out of Inuvik in the Northwest Territories of Canada, and the flights were directed into boundary layer and mid-level Arctic clouds. The NASA SLD flight research study (Miller et al. 1998)<sup>16</sup> was based out of Cleveland Ohio, with flights targeted at supercooled large drop (SLD) environments in the lower Great Lakes region. In total, there were 134 research flights undertaken during these five field campaigns including 81 with the National Research Council (NRC) Convair-580 and 53 with the NASA-Glenn Twin Otter. This represents approximately 400 hours of in-flight observations.

### III. Instrumentation

The instrumentation on each of the research aircraft was specifically oriented to be able to adequately measure icing and SLD environments including the drop distribution and liquid water content of the complete drop spectrum. Common instruments mounted on the Convair-580 aircraft during CFDE I, CFDE III, FIRE.ACE and AIRS I, and on the Twin Otter during the SLD flight research study and AIRS I, are listed in Table 2.

Table 2. Summary of instruments used to characterize icing and SLD environments.

NRC Convair-580 Aircraft	NASA-Glenn Twin Otter Aircraft
Rosemount temperature probe	Rosemount temperature probe
PMS King LWC probe (x2)	PMS King LWC probe
Nevzorov LWC/TWC probe	Nevzorov LWC/TWC probe
Goodrich Rosemount Icing Detector	Goodrich Rosemount Icing Detector
PMS FSSP 3-45 $\mu\text{m}$	
PMS FSSP 5-95 $\mu\text{m}$	PMS FSSP 5-95 $\mu\text{m}$
PMS 2D-C 25-800 $\mu\text{m}$ (mono probe)	
PMS 2D-G 25-1600 $\mu\text{m}$ (grey probe)	PMS 2D-G 15-960 $\mu\text{m}$ (grey probe)
PMS 2D-P 200-6400 $\mu\text{m}$ (mono probe)	

The King probes were used to measure LWC within  $\pm 15\%$  following King et al. (1985)<sup>17</sup>. Similarly, the Nevzorov LWC/TWC probes were used to measure the LWC and total water content (TWC) within  $\pm 15\%$  following Korolev et al. (1998)<sup>18</sup>. Calibrations, limitations and analysis techniques for the King and Nevzorov probes are provided in Cober et al. (1995)<sup>19</sup>, Cober et al. (2001)<sup>20</sup> and Strapp et al. (2003)<sup>21</sup>. The Rosemount Icing Detector was used to identify the presence of icing environments and to help segregate liquid, mixed and glaciated environments following the technique of Cober et al. (2001)<sup>20,22</sup>. The forward scattering spectrometer probe (FSSP) instruments were used to determine the sizes and concentrations of cloud drops over various diameter ranges. The error in measurement of droplet concentration and size has been estimated at  $\pm 20\%$  (Baumgardner 1983)<sup>23</sup> assuming that the optics are clean and adjusted correctly, that dead time and coincidence factors (Baumgardner et al. 1985)<sup>24</sup> have been corrected for, and that the effects of ice crystals have been interpreted correctly (Cober et al. 2001)<sup>20</sup>. The 2D cloud (2D-C and 2D-G) and 2D precipitation (2D-P) probes were used to measure shape, size and concentrations for cloud particles within their respective size ranges. The first four channels of each 2D probe were discarded because of depth of field uncertainties associated with these channels (Joe and List 1987<sup>25</sup>, Korolev et al. 1998<sup>26</sup>) and because of the significant sizing errors that occur in these channels (Korolev et al. 1998<sup>26</sup>). Strapp et al. (2001)<sup>27</sup> showed that distribution measurement errors for the 2D-C mono, when expressed as sizing errors, were  $< 10\%$  for particles  $\geq 5$  pixels (125  $\mu\text{m}$  for the MSC 2D-C probe). The hydrometeor images obtained with the 2D probes were processed following the centre-in technique of Heymsfield and Parrish (1978)<sup>28</sup>. This technique uses circular geometry computations that allow the effective photo-diode width to be at least a factor of two larger than the actual photo-diode width. The segregation of 2D particle images into drops and ice crystals is described by Cober et al. (2001)<sup>20</sup>. It should be noted that each aircraft also carried various additional instruments, which changed from project to project, including aerosol measuring probes, photographic equipment, icing cylinders, prototype SLD detectors, advanced cloud particle imaging probes, dew point hygrometers and others. However, since the latter instruments were not used in the extreme value analysis of icing conditions, they will not be discussed further.

### IV. Icing Environment Data Base

The data from each flight were averaged in sequential 30-s intervals, corresponding to a horizontal length scale of  $2.9 \pm 0.3$  km for the Convair-580 data and  $2.1 \pm 0.2$  km for the Twin Otter data. The error represents the standard deviation on the mean. The 30-s averaging scale was chosen because it represented a short averaging scale and a scale that generally allowed sufficient 2D measurements ( $> 100$ ) for statistical significance. The phase of each 30-s data point was determined following Cober et al. (2001)<sup>12</sup>. In order for a data point to be selected as an aircraft icing condition for the extreme value analysis, it had to have an average static temperature  $\leq 0^\circ\text{C}$ , an average LWC  $> 0.005$   $\text{g m}^{-3}$ , and the phase had to be assessed as being liquid phase

(i.e. there were no or minimal ice crystals observed) or mixed phase with ice crystal concentrations less than  $1 \text{ L}^{-1}$ . The latter threshold of  $1 \text{ L}^{-1}$  was selected following Cober et al. (2001)<sup>20</sup> in order to minimize the errors associated with misinterpreting ice crystal signals as water drops on the FSSP. For each aircraft icing environment observed, the entire FSSP spectrum, 2D-C spectrum  $\geq 5$  pixels ( $125 \mu\text{m}$ ) and 2D-P spectrum  $\geq 5$  pixels ( $1000 \mu\text{m}$  for the MSC instrument) were used to produce an integrated drop spectrum. The midpoint diameters of each FSSP and 2D bin were used to interpolate the normalized drop spectrum at 1-micron resolution, from 1 micron to the maximum drop diameter observed. The interpolation was based on a linear fit between logarithmic diameter and concentration pairs. FSSP and 2D channels were required to have 10 counts per 30-s interval before they were used in the analysis. When the number of counts per bin fell below 10, bins were combined until 10 counts were obtained. The spectra were truncated when there were fewer than 10 counts in sizes larger than the last useful bin. The maximum drop diameter ( $D_{\text{max}}$ ) for each spectrum was assessed as the mid-point of the last useful bin. Each icing data point with a temperature  $\leq 0^\circ\text{C}$  and with at least one measurement bin of drops larger than  $100 \mu\text{m}$  in diameter was considered as a SLD environment. For each such SLD environment the  $1 \mu\text{m}$  drop spectrum was used to compute the median volume diameters. The analysis of SLD drop spectra is described in Cober et al. (2003)<sup>29</sup>.

In total, there were 48301 30-s in-flight data points collected during the five flight campaigns. Of these, 27497 (57%) data points were assessed as being in-cloud with a TWC  $> 0.005 \text{ g m}^{-3}$ . There were 22263 in-cloud observations (46% of in-flight) with an average static temperature  $\leq 0^\circ\text{C}$ , and 14199 observations (29% of in-flight) where supercooled liquid water was assessed to exist. There were 9808 in-cloud in-icing data points with ice crystal concentrations less than  $1 \text{ L}^{-1}$  where the drop spectra could be accurately determined. Of these, there were 2444 observations with an average static temperature  $\leq 0^\circ\text{C}$ , an average LWC  $> 0.005 \text{ g m}^{-3}$ , an ice crystal concentration  $< 1 \text{ L}^{-1}$ , an assessment of either liquid or mixed phase, and  $D_{\text{max}} > 100 \mu\text{m}$  in diameter. The latter data points, which represent 5% of the in-flight observations, represent the SLD data base. The extreme value analysis will be applied both to the aircraft icing data with drops  $< 100 \mu\text{m}$  in diameter (7364 observations) and to the SLD data (2444 observations).

The SLD data were sub-divided into four subsets that physically represented icing environments which contained different relative sizes and mass fractions of SLD. This approach followed that suggested by Shah et al. (2000)<sup>30</sup> and further developed by Cober et al. (2003)<sup>29</sup>. The four subsets were designed to provide a standard to support the aviation industry in its attempts to develop certification tools and standards for SLD icing conditions. In order to conduct realistic wind tunnel or numerical icing simulation experiments that mimic cloud environments that contain SLD, it was considered necessary to characterize the data in a form that was both practical and realistic. Practical implies a minimum number of representative drop spectra, while realistic implies that a wide range of natural icing conditions should be included in the characteristic spectra. The environments are summarized in Table 3.

Table 3. Four subsets of SLD conditions.

Definition	Median Volume Diameter (MVD)	Maximum Drop Diameter ( $D_{\text{max}}$ )	Number of data points
SLD icing environments with freezing drizzle (ZLE)	$< 40 \mu\text{m}$	100-500 $\mu\text{m}$	1469
SLD icing environments with freezing drizzle (ZLE)	$> 40 \mu\text{m}$	100-500 $\mu\text{m}$	335
SLD icing environments with freezing rain (ZRE)	$< 40 \mu\text{m}$	$> 500 \mu\text{m}$	193
SLD icing environments with freezing rain (ZRE)	$> 40 \mu\text{m}$	$> 500 \mu\text{m}$	447

The SLD environments are designed to represent any icing environment that has drops larger than  $100 \mu\text{m}$  in diameter. These environments may or may not contain drops smaller than  $100 \mu\text{m}$ . The SLD conditions are distinct from those described in FAR 25-C Appendix C because the FAR 25-C conditions are assumed to have maximum drop diameters  $< 100 \mu\text{m}$ . This assumption will not always be correct because the FAR 25-C data were based on icing cylinder measurements from which MVD values  $> 40 \mu\text{m}$  could not be accurately determined, and since they were not able to directly observe SLD drops. However, based on the large data base of in-situ measurements obtained in this study, this assumption is likely to be generally correct.

## V. Extreme Value Analysis of Icing Data

A comparison of the observed aircraft icing environments with the icing envelopes for continuous maximum icing from FAR 25-C is shown in Figure 1. The data only include those observations where  $D_{max} < 100 \mu\text{m}$ . Since the FAR 25-C curves represent continuous maximum icing conditions for horizontal extents of 17.4 n mi (32.2 km), the 30-s data were adjusted to 32.2 km using the distance scale factor described in section VII. The number of data points for each temperature range ( $T_a$ ) is also listed in the legend to Figure 1. In general the FAR 25-C curves bound the data fairly well except in the areas smaller than  $15 \mu\text{m}$  and larger than  $40 \mu\text{m}$  where the FAR 25-C curves did not extend.

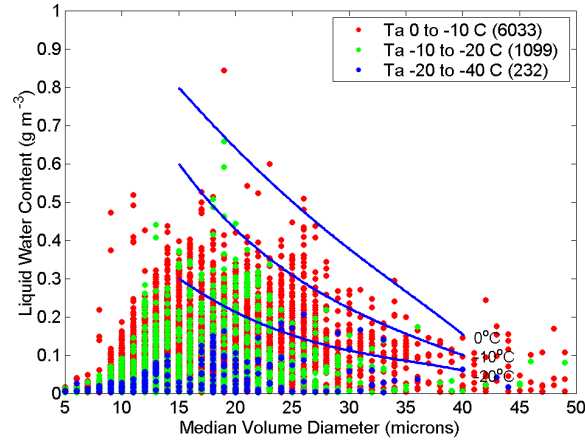


**Figure 1. Comparison of the 30-s in-situ data with the FAR 25-C icing envelopes. The FAR 25-C envelopes for 0, -10 and -20°C are shown as solid blue curves. The LWC values have been scaled from 3 km to 32.2 km in order to be consistent with the FAR 25-C curves.**

The in-situ aircraft icing data were analysed using the EVIM extreme value analysis software described by Gencay et al. (2002)<sup>8</sup>. The method of fitting the data to the EVD and of estimating the shape of the tail of the distribution will be described below. Similar to Lewis and Bergrun (1952)<sup>3</sup> and Masters (1984)<sup>5</sup> the data were segregated into MVD bins. Figure 2 shows the ordered empirical distribution of the 1252 data points with MVD between 20 and 25  $\mu\text{m}$ . There was no segregation of the data by temperature for the extreme value analysis.

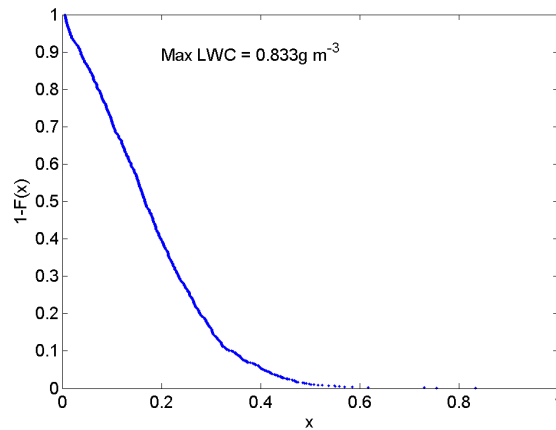


**Figure 2. Ordered empirical distribution plot of the LWC (x) data for MVD between 20 and 25  $\mu\text{m}$ . The largest LWC observed in the distribution is  $0.83 \text{ g m}^{-3}$ .**

Following Gencay et al. (2002)<sup>8</sup> the shape of the tail of the distribution is estimated as a function of the threshold (exceedance value) by fitting the data to a generalized Pareto distribution. Figure 3 shows an

estimate of the shape function for all possible thresholds and an expansion of the shape function for exceedances above point 1160 to point 1252. Point 1160 had a LWC of  $0.32 \text{ g m}^{-3}$ . If the threshold of the final analysis was selected at point 1160, then the tail of the distribution would be fitted using only the 92 observations with  $\text{LWC} > 0.32 \text{ g m}^{-3}$ .

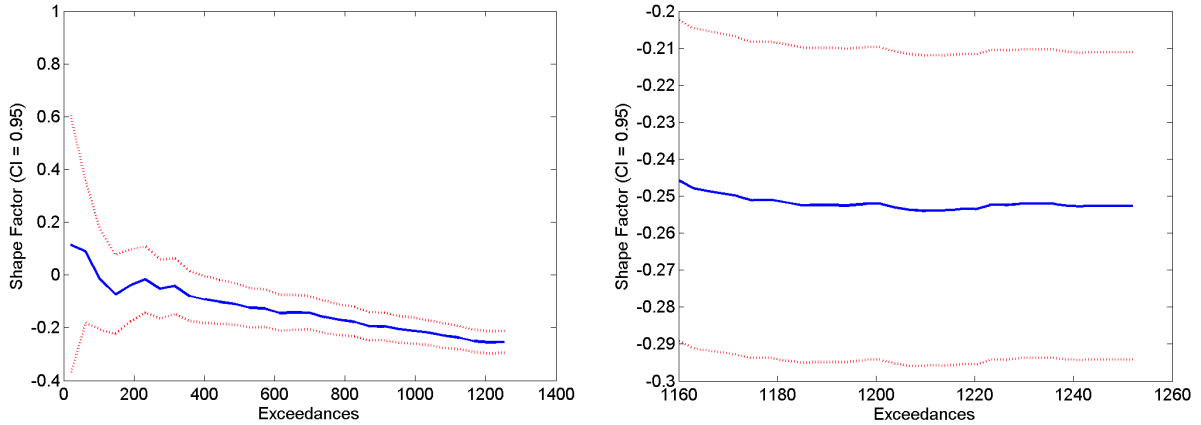


**Figure 3. Plots of the shape factor of the LWC data distribution for MVD between 20 and 25  $\mu\text{m}$  for all thresholds (left) and for thresholds above data point 1160. The red curves represent the 95% confidence limits for this fit.**

Since the shape factor seems quite stable above a threshold of  $0.32 \text{ g m}^{-3}$  (point 1160), this was selected at the threshold value for fitting the data to the generalized Pareto distribution. This yielded a shape parameter of  $-0.03 \pm 0.09$  and a scale parameter of  $0.08 \pm 0.01$ . These values were then used to fit the tail of the distribution and to estimate the 99 and 99.9% probabilities within 95% confidence limits as shown in Figure 4. The uncertainty associated with the probability estimates increase significantly for lower probability events.

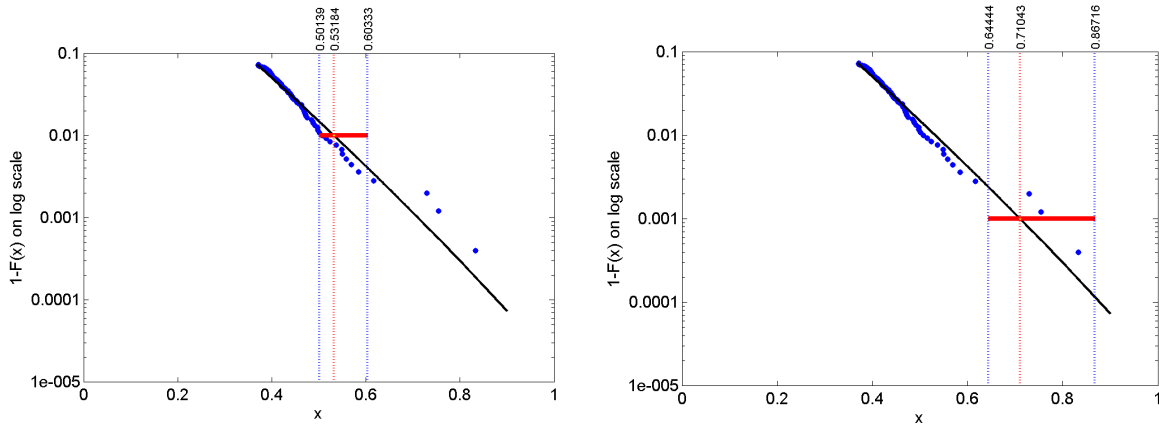


**Figure 4. Estimation of the 99% or  $1-F(x) = 0.01$  (left) and 99.9% or  $1-F(x) = 0.001$  (right) probability values for LWC ( $x$ ) with 95% confidence limits, by fitting the tail of the LWC distribution to a generalized Pareto distribution. The data are shown as blue dots and the fit is shown as a black line. The 95% confidence limits are shown as a red bar. The values of LWC associated with the best fit probability value and the associated 95% confidence limits are shown along the top axis of each plot.**

Sensitivity studies were undertaken to determine whether the selection of different thresholds would give significantly different 99 and 99.9% probability values. The probability estimates and the 95% confidence limits were generally quite similar which is consistent with the observations that the shape

factors (Figure 3) were in general relatively stable above some threshold value. A similar analysis was done for several MVD bins between 5 and 50  $\mu\text{m}$ . The shape parameters varied between  $0 \pm 0.1$  and  $-0.4 \pm 0.2$  which suggests that the distribution tails are narrow and are of the Weibull family. Figure 5 shows the extreme value analysis for 99% and 99.9% exceedance probabilities for each of the MVD bins. The 99 and 99.9% probabilities were also computed using the gamma, Weibull and exponential distributions and the results are shown for comparison. The FAR 25-C curves were assessed as representing 99.9% LWC envelopes by Lewis and Bergrun (1952)<sup>3</sup>. The 0°C curve agrees quite well with the 99.9% extreme value analysis between 20 and 35  $\mu\text{m}$ . The errors in measuring LWC with multiple icing cylinders increase with decreasing drop size below 20  $\mu\text{m}$  because of the high slope of the collision efficiency curve in that region. That is presumably why the FAR 25-C curves do not extend below 15  $\mu\text{m}$ . Similarly, the errors in determining MVD with multiple icing cylinders increase with increasing drop size above 40  $\mu\text{m}$  because of the flattening of the collision efficiency curves in this region. Considering these errors, the agreement between the EVD and the FAR 25-C curves is quite remarkable. The results in Figure 5 indicate that fitting the LWC distributions to exponential, gamma or Weibull distributions would overestimate the 99 and 99.9% LWC values, although the Weibull distribution fit tended to agree with the EVD within the 95% confidence limits. The FAR 25-C LWC envelopes were fit to the Gumbel family of curves (shape factor = 0), hence the FAR 25-C fits may have overestimated the extreme LWC values.

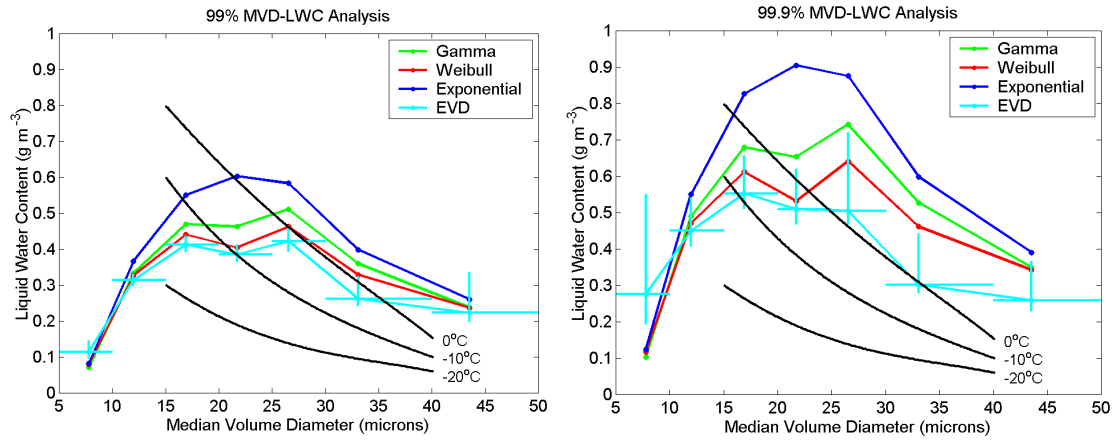


**Figure 5. Analysis of the 99% (left) and 99.9% (right) probability curves for LWC using an EVD, as well as Weibull, gamma and exponential distributions. The FAR 25-C curves for 0, -10 and -20°C are also shown for comparison. The 99 and 99.9% LWC values were scaled to a horizontal distance of 32.2 km. The 95% confidence limits for the analysis of the EVD are shown as error bars along the y axis. The error bars along the x axis show the MVD bins that were used.**

## VI. Extreme Value Analysis of SLD Data

The number of data points at 30-s resolution for the four SLD subsets ranged from 193 to 1469. In order to maximize the number of data points used in the analysis no further subdividing of the SLD subsets (i.e. as a function of temperature or MVD) was undertaken. Table 4 shows, for each SLD subset, the threshold values that were used when fitting the data to a generalized Pareto distribution. Table 4 also shows the maximum observed LWC, the LWC corresponding to the threshold selection and the shape factor determined for each fit.

Table 4. Threshold characteristics for the EVD for each SLD environment.

SLD Environment	Number Points	Threshold Point	Threshold LWC (g m <sup>-3</sup> )	Maximum LWC (g m <sup>-3</sup> )	Shape Factor $\xi \pm \sigma$
ZLE MVD < 40 $\mu\text{m}$	1469	1375	0.39	0.77	$-0.04 \pm 0.10$
ZLE MVD > 40 $\mu\text{m}$	335	300	0.20	0.39	$-0.28 \pm 0.14$
ZRE MVD < 40 $\mu\text{m}$	193	150	0.17	0.49	$-0.14 \pm 0.11$
ZRE MVD > 40 $\mu\text{m}$	447	410	0.19	0.41	$-0.09 \pm 0.14$

The standard deviation ( $\sigma$ ) for each shape factor is listed in Table 4. The shape factors were fairly similar and generally agreed within their standard deviations. The shape factors suggested narrow tailed distributions. The 99 and 99.9% LWC values were estimated for each of the four SLD environments. The fits along with the 99.9% estimates and 95% confidence limits are shown in Figure 6 for each SLD environment.

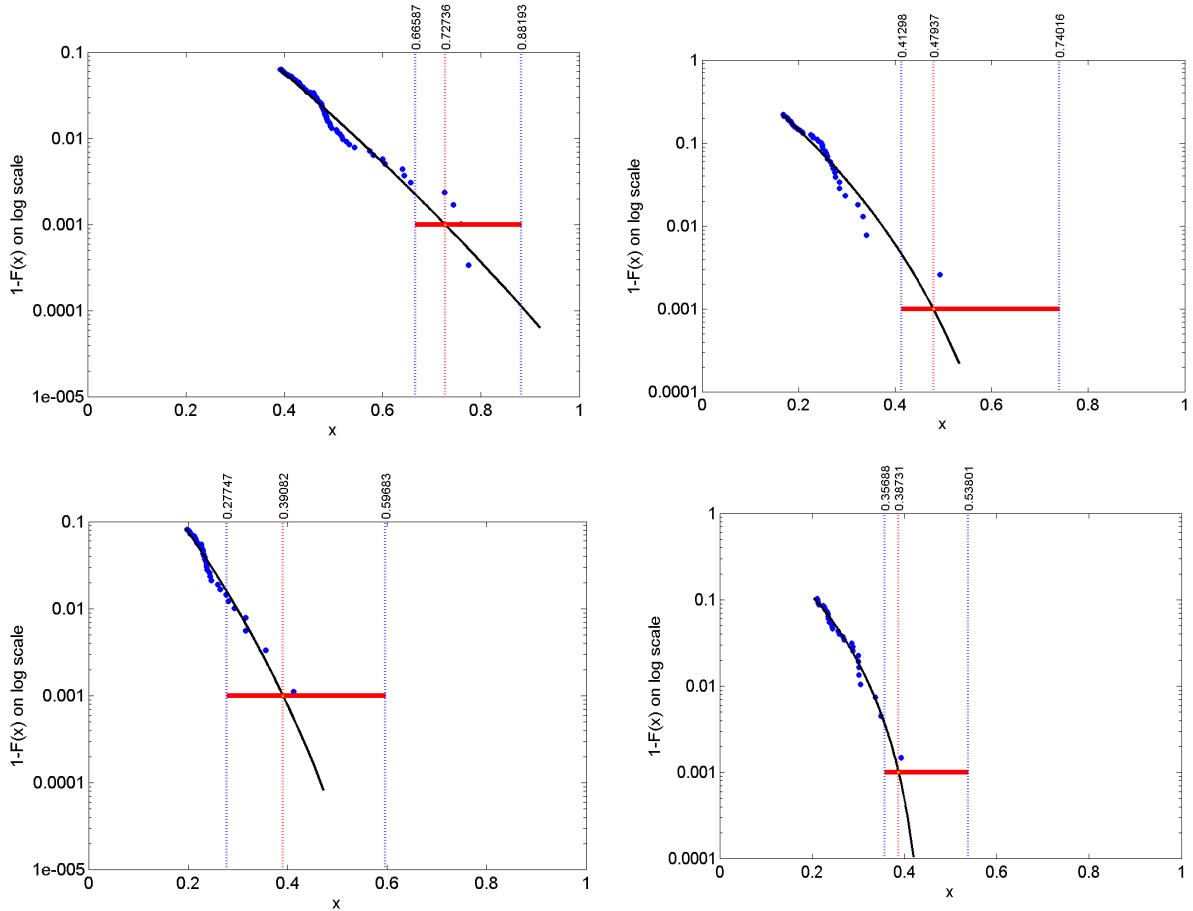


**Figure 6. Estimation of the 99.9% or  $1-F(x) = 0.001$  probability values for each SLD environment for LWC ( $x$ ) with 95% confidence limits, by fitting the tail of the LWC distribution to a generalized Pareto distribution. The data are shown as blue dots and the fit is shown as a black line. The 95% confidence limits are shown as a red bar. The values of LWC associated with the best fit probability value and the associated 95% confidence limits are shown along the top axis of each plot. Top left (ZLE MVD < 40  $\mu\text{m}$ ), top right (ZLE MVD > 40  $\mu\text{m}$ ), bottom left (ZRE MVD < 40  $\mu\text{m}$ ), bottom right (ZRE MVD > 40  $\mu\text{m}$ ).**

Sensitivity studies were done with different threshold values to ensure that the choice of threshold did not significantly influence the results. There were no observations of SLD environments that had a probability that was lower than the upper 95% confidence limit of the 99.9% LWC value ( $1-F(x) = 0.001$ ). The 99.9% LWC values have significant uncertainty which is related to the limited number of extreme (i.e. above 99%) LWC environments observed. Regardless, the fits shown in Figure 6 appear to represent the observations quite well.

The SLD icing environments observed are shown in Figure 7 as a function of LWC and MVD. Each data point represents a 30-s observation. The data are segregated by  $D_{\text{max}}$  and MVD into the four SLD environments described in Table 4. The Newton (1978)<sup>9</sup> potential accumulation envelopes for 1, 6 and 12  $\text{g cm}^{-2} \text{h}^{-1}$  are also shown for comparison. Note that the 30-s data have not been scaled to a horizontal scale of 32.2 km in Figure 7. The 99 and 99.9% LWC values and their 95% confidence limits are also shown for each of the four SLD environments in Figure 7.

The 99% and 99.9% LWC values obtained from the extreme value analysis are compared with those obtained from gamma, exponential and Weibull distributions in Figure 8. The exponential distribution always overestimates the extreme values in comparison to the EVD. Conversely the Weibull distribution generally agrees with the EVD within the 95% confidence limits.

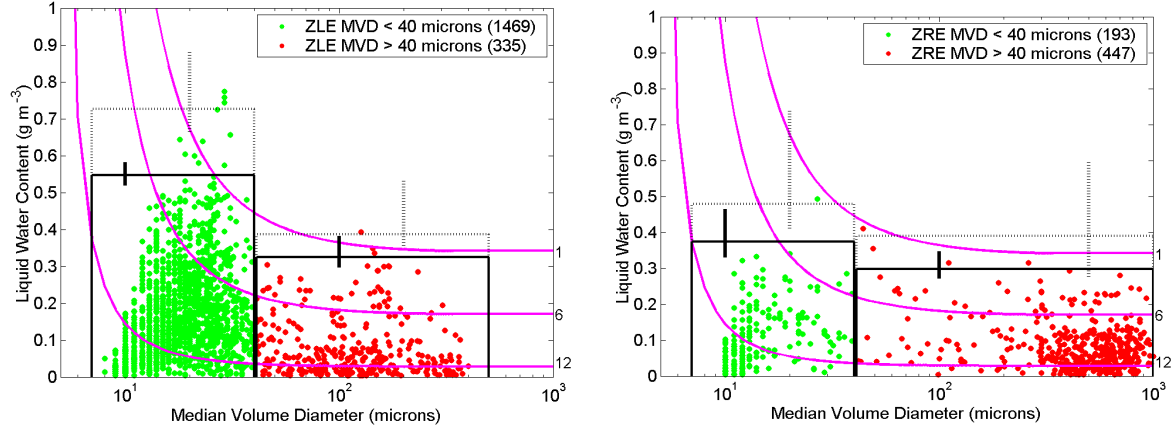


**Figure 7. Plot of MVD and LWC for each observed SLD icing environment at 30-s resolution. The 99% LWC values are shown by the solid black lines. The range of the 95% confidence limits are shown by the error bar on the horizontal black lines. The 99.9% LWC values and their 95% confidence limits are represented by dashed black lines. The potential accumulation envelopes described by Newton (1978)<sup>9</sup> for 1, 6 and 12 g cm<sup>-2</sup> h<sup>-1</sup> are represented by the magenta curves. SLD environments with freezing drizzle (ZLE) are on the left figure, while those with freezing rain (ZRE) are on the right figure.**

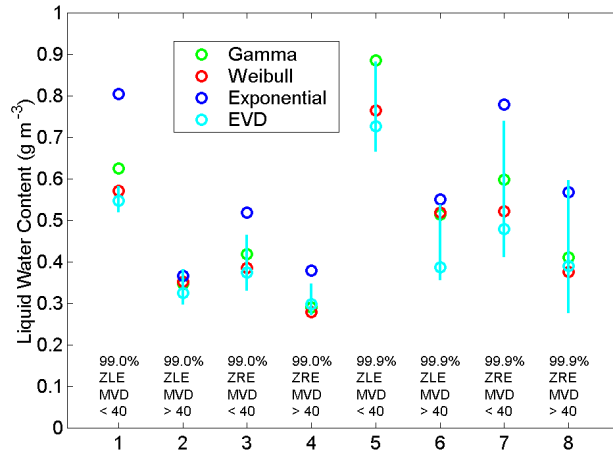


**Figure 8. Comparison of the 99 and 99.9 LWC values obtained from the EVD, gamma, exponential and Weibull distributions for each SLD environment.**

### VII. Distance Scale Factor

The in-situ data were analysed at 30-s resolution which represented a horizontal length scale of approximately 3 km. The FAR 25-C envelopes were derived for a horizontal length scale of 17.4 n mi. FAR 25-C provided a scale factor for conversion of any horizontal length scales larger than 5 n mi to the standard length scale of 17.4 n mi. In order to determine a similar scale factor for the in-situ data used in this study, the data were analysed at 60-s, 120-s and 300-s resolution corresponding to horizontal scales of approximately 6, 12 and 30 km respectively. For the determination of scale factor, the data were not

segregated by temperature or MVD. Figure 9 shows the 99% and 99.9% LWC values as a function of horizontal extent for all data with  $D_{max} < 100 \mu\text{m}$  in diameter. For the 99% LWC distribution, the dimensionless scale factor (SF) is defined from the best fit by setting the value of  $SF = 1$  for a horizontal extent of 17.4 n mi within the following equation:

$$LWC_{dh} = LWC_{32} * SF \quad (7)$$

$$SF = \left(\frac{1}{0.370}\right) * [0.584 - 0.141 \log_{10}(d_h)] = 1.58 - 0.38 \log_{10}(d_h) \quad (8)$$

where  $LWC_{32}$  is the LWC value at 32.2 km, SF is the scale factor,  $d_h$  is the distance in km and  $LWC_{dh}$  is the LWC at a horizontal length scale of  $d_h$ . The value of SF for the 99.9% LWC distribution is given by:

$$SF = \left(\frac{1}{0.501}\right) * [0.804 - 0.200 \log_{10}(d_h)] = 1.60 - 0.40 \log_{10}(d_h) \quad (9)$$

which agrees very well with the SF for the 99% LWC distribution. The scale factors for the 99% and 99.9% LWC distributions are also shown in Figure 9 and are compared to the scale factor from FAR 25-C. The FAR 25-C slope is significantly steeper. This may be related to the distribution type that the FAR 25-C data were fitted to. When the 99% and 99.9% LWC data were fitted to exponential distributions, the corresponding scale factors were within 8% of the FAR 25-C scale factor. The FAR 25-C data were fitted to the Gumbel family of distributions (of which the exponential distribution is one type) which have shape factors of 0. The analysis of the in-situ data with EVD has shown that the shape factors are slightly negative and that analysis with distributions within the Gumbel family would overestimate the LWC values.

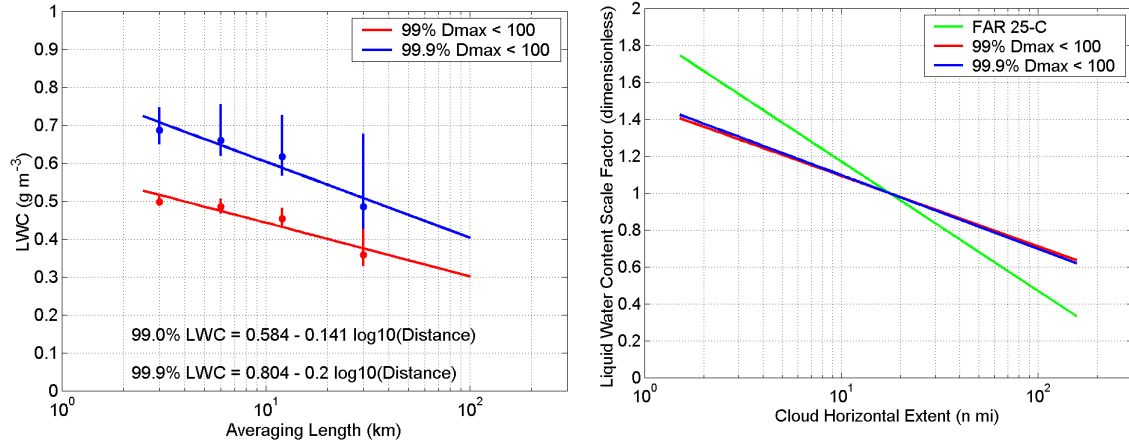


**Figure 9. Analysis of the 99% and 99.9% (left) LWC values for all icing observations with  $D_{max} < 100 \mu\text{m}$  as a function of horizontal extent. The error bars represent the 95% confidence limits computed from the EVD. The best fits are shown on each graph. The dimensionless scale factors (SF) for the 99% and 99.9% LWC distributions are compared with the scale factor from FAR 25-C on the right plot.**

At 120-s and 300-s resolution, there were fewer than 100 observations for several of the four SLD environments. This made the analysis of extreme LWC values difficult because there were fewer data points for fitting the tail of the distribution, which tended to significantly increase the uncertainty of the fits. In order to mitigate this, all of the SLD data were combined in order to attempt to determine a single scale factor equation which would represent each of the four SLD environments. Figure 10 shows the 97%, 99% and 99.9% LWC values as a function of horizontal extent for the collective SLD environments as well as the corresponding dimensionless scale factors.

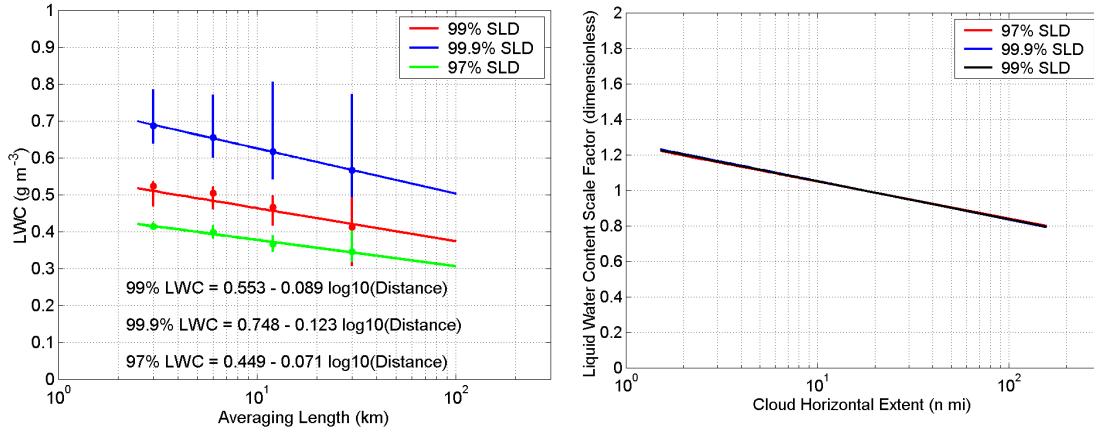


**Figure 10. Analysis of the 97%, 99% and 99.9% (left) LWC values for all SLD observations as a function of horizontal extent. The error bars represent the 95% confidence limits computed from the extreme value analysis. The best fits are shown on each graph. The dimensionless scale factors (SF) for each of these distributions are shown on the right plot.**

The scale factor for the 99% SLD LWC distribution is given by:

$$SF = \left(\frac{1}{0.418}\right) * [0.553 - 0.089 \log_{10}(d_h)] = 1.32 - 0.21 \log_{10}(d_h) \quad (10)$$

The three scale factors agree within 5%. The 95% confidence limits for the 99 and 99.9% data are such that a significantly more horizontal curve could be fitted to this data. However the 97% LWC data have much smaller uncertainty limits suggesting that the scale factor is acceptable. The only way to reduce the uncertainty of the fit would be to significantly increase the size of the in-situ data base. Figure 11 shows how well this single equation fit the individual SLD environments. The uncertainties in Figure 11 are significantly higher because of the small number of data points used in some of the fits. Regardless, each of the four SLD environments seems to be well represented by Equation 10.

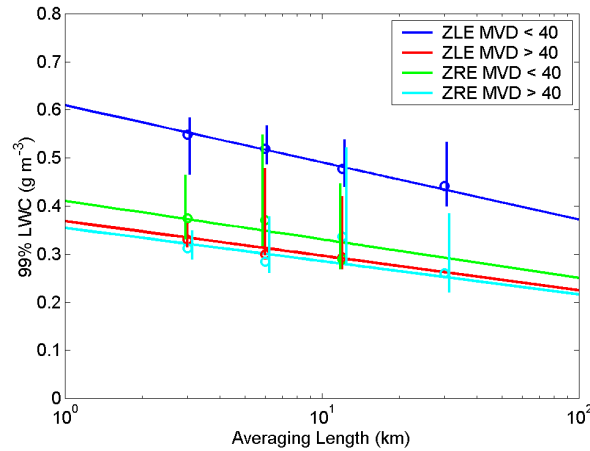


**Figure 11. Plot of the 99% LWC values as a function of horizontal extent for each of the four SLD environments. The four curves were based on Equations 7 and 10 with different values of LWC<sub>32</sub>.**

## VIII. Conclusions

Based on a statistical analysis of 9808 in-situ aircraft icing observations made at 30-s resolution, of which 2444 had supercooled large drops > 100 μm in diameter, the following conclusions were obtained:

1. For icing conditions with drops  $< 100 \mu\text{m}$  in diameter, the 99.9% LWC values derived using extreme value analysis techniques are consistent with the FAR 25-C 99.9% envelopes for continuous maximum icing conditions for MVD values in the range 20-35  $\mu\text{m}$ . The FAR 25-C envelopes overestimate the 99.9% LWC values for MVD  $< 20 \mu\text{m}$  and underestimate the 99.9% LWC values for MVD  $> 35 \mu\text{m}$ . These differences are likely related to the errors in LWC and MVD determination with multiple icing cylinders which are largest for low values of drop collision efficiency (i.e.  $< 20 \mu\text{m}$ ) where the collision efficiency curve has an extremely steep slope, and for constant values of drop collision efficiency (i.e.  $> 35 \mu\text{m}$ ) where the collision efficiency curves are levelling off.
2. When the icing conditions with drops  $< 100 \mu\text{m}$  in diameter are fitted to an exponential distribution, the dimensionless scale factor derived for computing horizontal extent agrees with the FAR 25-C dimensionless scale factor within 8%. However, when the data are fitted to an extreme value distribution, the scale factor has a significantly lower slope. It is suggested that the FAR 25-C dimensionless scale factor is biased by the distributions used for fitting the 99.9% LWC values and will underestimate the LWC for long horizontal extents.
3. The 99% and 99.9% LWC values were determined for four subsets of icing conditions associated with SLD environments with drops  $> 100 \mu\text{m}$  in diameter. Such an analysis has not been previously reported. The extreme LWC values were computed using an extreme value distribution and compared with fits from exponential, gamma and Weibull distributions. In general, the latter fits overestimated the LWC values relative to the EVD, although the Weibull distribution fits tended to agree within the 95% confidence limits. The EVD fits indicated that the LWC distribution had a slightly negative shape factor which is indicative of a narrow distribution with a sharp cut off. A dimensionless scale factor for SLD conditions was derived which showed a significantly lower slope than that derived for the icing conditions with drops  $< 100 \mu\text{m}$ . The LWC values and dimensionless scale factor for SLD conditions provides an analogous (to FAR 25-C) and supplementary ( $> 40 \mu\text{m}$ ) characterization of extreme icing environments.
4. The 99% and 99.9% LWC values derived from the in-situ data using extreme value analysis gave significantly different results than those obtained by fitting the LWC data to other more common distributions. Since extreme value statistical analysis allows quantification of the nature of distributions in the tails of the distributions, and hence provides a more accurate method for determining extreme values, it is suggested that it be used when developing future envelopes in support of aircraft certification programs.

### **Acknowledgments**

Funding for this work was provided by Environment Canada, NASA-Glenn, National Research Council of Canada, Federal Aviation Administration, Transport Canada and the National Search and Rescue Secretariat of Canada. The authors would like to acknowledge Walter Strapp and Alexei Korolev of MSC, Dave Marcotte of NRC and Tom Ratvasky of NASA for their contributions to collecting the data.

### **References**

1. Federal Aviation Administration, 1999: U.S. Code of Federal Regulations, Title 14 (Aeronautics and Space), Part 25 (Airworthiness Standard: Transport Category Airplanes), Appendix C, Office of the Federal Register, National Archives and Records Administration, U.S. Government Printing Office, Washington D.C., 20402-9328.
2. Jones, A.R., and W. Lewis, 1949: Recommended values of meteorological factors to be considered in the design of aircraft ice-prevention equipment. National Advisory Committee for Aeronautics, Technical Note 1855, 14 pp.
3. Lewis, W., and N.R. Bergrun, 1952: A probability analysis of the meteorological factors conducive to aircraft icing in the United States. NACA Technical Note No. 2738, Washington, 93 pp.
4. Gumbel, E.J., 1942: On the frequency distribution of extreme values in meteorological data. *Bull. Amer. Met. Soc.*, **23**, 95-105.
5. Masters, C.O., 1984: A new characterization of supercooled cloud design for aircraft ice protection systems below 10,000 ft. AGL. *AIAA 22nd Aerospace Sci. Meeting and Exhibit*, Reno, Nevada, 9-12 January 1984, AIAA 84-0182.
6. Coles, S., 2001: An introduction to statistical modeling of extreme values. Springer, 205 pp.
7. Fisher, R.A., and L.H.C. Tippett (1928): Limiting forms of the frequency distribution of the largest or smallest members of a sample. *Proc. Cambridge Phil. Soc.*, **24**, 180-190.

8. Gencay, R., F. Selcuk, and A. Ulugulyagci, 2002: EVIM: A software package for extreme value analysis in MATLAB. *Studies in Nonlinear Dynamics and Econometrics*, **5**, 213-239.
9. Newton, D.W., 1978: An integrated approach to the problem of aircraft icing. *J. Aircraft*, **15**, 374-380.
10. Isaac, G.A., S.G. Cober, A.V. Korolev, J.W. Strapp, A. Tremblay, and D.L. Marcotte, 1999: Canadian Freezing Drizzle Experiment. *AIAA 37th Aerospace Sci. Meeting and Exhibit*, Reno Nevada, 11-14 January 1999.
11. Isaac, G.A., S.G. Cober, J.W. Strapp, A.V. Korolev, A. Tremblay, and D.L. Marcotte, 2001a: Recent Canadian research on aircraft in-flight icing. *Canadian Aeronautics and Space Journal*, **47**, 213-221.
12. Cober, S.G., G.A. Isaac, and J.W. Strapp, 2001a: Characterizations of aircraft icing environments that include supercooled large drops. *J. Appl. Meteor.*, **40**, 1984-2002.
13. Isaac, G.A., S.G. Cober, J.W. Strapp, D. Hudak, T.P. Ratvasky, D.L. Marcotte, and F. Fabry 2001b: Preliminary results from the Alliance Icing Research Study (AIRS). *AIAA 39th Aerospace Sci. Meeting and Exhibit*, Reno Nevada, 8-11 January 2001, AIAA 2001-0393.
14. Cober, S.G., T.P. Ratvasky, and G.A. Isaac, 2002: Assessment of aircraft icing conditions observed during AIRS. *AIAA 40th Aerospace Sci. Meeting and Exhibit*, Reno Nevada, 14-17 January 2002, AIAA 2002-0674.
15. Curry, J.A., P.V. Hobbs, M.D. King, D.A. Randall, P. Minnis, G.A. Isaac, J.O. Pinto, T. Uttal, A. Bucholtz, D.G. Cripe, H. Gerber, C.W. Fairall, T.J. Garrett, J. Hudson, J.M. Intrieri, C. Jakob, T. Jensen, P. Lawson, D. Marcotte, L. Nguyen, P. Pilewskie, A. Rangno, D. Rogers, K.B. Strawbridge, F.P.J. Valero, A.G. Williams, and D. Wylie, 2000: FIRE Arctic Clouds Experiment. *Bull. Amer. Meteor. Soc.*, **81**, 5-29.
16. Miller, D., T. Ratvasky, B. Bernstein, F. McDonough, and J.W. Strapp, 1998: NASA/FAA/NCAR supercooled large droplet icing flight research: Summary of winter 96-97 flight operations. *AIAA 36th Aerospace Sci. Meeting and Exhibit*, Reno, Nevada, 12-15 January 1998, AIAA 98-0577.
17. King, W.D., J.E. Dye, J.W. Strapp, D. Baumgardner, and D. Huffman, 1985: Icing wind tunnel tests on the CSIRO liquid water probe. *J. Atmos. Oceanic Technol.*, **2**, 340-352.
18. Korolev, A.V., J.W. Strapp, G.A. Isaac, and A.N. Nevzorov, 1998a: The Nevzorov airborne hot-wire LWC-TWC probe: Principles of operation and performance characteristics. *J. Atmos. Oceanic Tech.*, **15**, 1495-1510.
19. Cober, S.G., G.A. Isaac, and J.W. Strapp, 1995: Aircraft icing measurements in east coast winter storms. *J. Appl. Meteor.*, **34**, 88-100.
20. Cober, S.G., G.A. Isaac, A.V. Korolev, and J.W. Strapp, 2001: Assessing cloud-phase conditions. *J. Appl. Meteor.*, **40**, 1967-1983.
21. Strapp, J.W., J. Oldenburg, R. Ide, L. Lilie, S. Bacic, Z. Vukovic, M. Oleskiw, D. Miller, E. Emery, and G. Leone, 2003: Wind tunnel measurements of the response of hot-wire liquid water content instruments to large droplets. *J. Atmos. Oceanic Technol.*, **20**, 791-806.
22. Cober, S.G., G.A. Isaac, and A.V. Korolev, 2001: Assessing the Rosemount icing detector with in-situ measurements. *J. Atmos. Oceanic Technol.*, **18**, 515-528.
23. Baumgardner, D., 1983: An analysis and comparison of five water droplet measuring instruments. *J. Climate Appl. Meteor.*, **22**, 891-910.
24. Baumgardner, D., W. Strapp, and J.E. Dye, 1985: Evaluation of the forward scattering spectrometer probe. Part II: Corrections for coincidence and dead time losses. *J. Atmos. Oceanic Technol.*, **2**, 626-632.
25. Joe, P., and R. List, 1987: Testing and performance of two-dimensional optical array spectrometers with greyscale. *J. Atmos. Oceanic Technol.*, **4**, 139-150.
26. Korolev, A.V., J.W. Strapp, and G.A. Isaac, 1998b: Evaluation of the accuracy of PMS optical array probes. *J. Atmos. Oceanic Technol.*, **15**, 708-720.
27. Strapp, J.W., F. Albers, A. Reuter, A.V. Korolev, W. Maixner, E. Rashke, and Z. Vukovic, 2001: Laboratory measurements of the response of a PMS OAP-2DC probe. *J. Atmos. Oceanic Technol.*, **18**, 1150-1170.
28. Heymsfield, A.J., and J.L. Parrish, 1978: A computational technique for increasing the effective sampling volume of the PMS two-dimensional particle size spectrometer. *J. Appl. Meteor.*, **17**, 1566-1572.
29. Cober, S.G., G.A. Isaac, A.D. Shah, and R. Jeck, 2003: Defining characteristic cloud drop spectra from in-situ measurements. *AIAA 41st Aerospace Sci. Meeting and Exhibit*, Reno Nevada, 6-10 January 2003, AIAA 2003-0561.
30. Shah, A.D., M.W. Patnoe, and E.L. Berg, 2000: Engineering analysis of the atmospheric icing environment including large droplet conditions. *Society of Automotive Engineers*, 2000-01-2115.